

## Article

# An Optimized Method for 3D Magnetic Navigation of Nanoparticles inside Human Arteries

Evangelos Karvelas <sup>1</sup>, Christos Liosis <sup>1</sup> , Andreas Theodorakakos <sup>2</sup>, Ioannis Sarris <sup>2</sup>  and Theodoros Karakasidis <sup>1,3,\*</sup> 

<sup>1</sup> Department of Civil Engineering, University of Thessaly, Pedion Areos, 38221 Volos, Greece; karvelas@uth.gr (E.K.); cliosis@uth.gr (C.L.)

<sup>2</sup> Department of Mechanical Engineering, University of West Attica, Thivon 250, 12241 Aigaleo, Greece; atheod@uniwa.gr (A.T.); sarris@uniwa.gr (I.S.)

<sup>3</sup> Department of Physics, School of Science, University of Thessaly, 35100 Lamia, Greece

\* Correspondence: thkarak@uth.gr; Tel.: +30-242-107-4163

**Abstract:** A computational method for optimum magnetic navigation of nanoparticles that are coated with anticancer drug inside the human vascular system is presented in this study. For this reason a 3D carotid model is employed. The present model use Computational Fluid Dynamics (CFD) and Discrete Element Method (DEM) techniques along with Covariance Matrix Adaptation (CMA) evolution strategy for the evaluation of the optimal values of the gradient magnetic field. Under the influence of the blood flow the model evaluates the effect of different values of the gradient magnetic field in order to minimize the distance of particles from a pre-described desired trajectory. Results indicate that the diameter of particles is a crucial parameter for an effective magnetic navigation. The present numerical model can navigate nanoparticles with diameter above 500 nm with an efficiency of approximately 99%. It is found that the velocity of the blood seems to play insignificant role in the navigation process. A reduction of 25% in the inlet velocity leads the particles only 3% closer to the desired trajectory. Finally, the computational method is more efficient as the diameter of the vascular system is minimized because of the weak convective flow. Under a reduction of 50% in the diameter of the carotid artery the computational method navigate the particles approximately 75% closer to the desired trajectory. The present numerical model can be used as a tool for the determination of the parameters that mostly affect the magnetic navigation method.

**Keywords:** nanoparticles; Computational Fluid Dynamics (CFD); Discrete Element Method (DEM); Covariance Matrix Evolution Strategy (CMAES); magnetic navigation; drug delivery



**Citation:** Karvelas, E.; Liosis, C.; Theodorakakos, A.; Sarris, I.; Karakasidis, T. An Optimized Method for 3D Magnetic Navigation of Nanoparticles inside Human Arteries. *Fluids* **2021**, *6*, 97. <https://doi.org/10.3390/fluids6030097>

Academic Editor: Pavel S. Berloff

Received: 8 January 2021

Accepted: 18 February 2021

Published: 1 March 2021

**Publisher's Note:** MDPI stays neutral with regard to jurisdictional claims in published maps and institutional affiliations.



**Copyright:** © 2021 by the authors. Licensee MDPI, Basel, Switzerland. This article is an open access article distributed under the terms and conditions of the Creative Commons Attribution (CC BY) license (<https://creativecommons.org/licenses/by/4.0/>).

## 1. Introduction

Nowadays, chemotherapy is one of the most often used techniques against tumour cells. In this method, anticancer drug such as doxorubicin is injected into the human vascular system. This method results in severe toxic side-effects as the drug affects both cancer and healthy cells. In order to overcome the side-effects of the drugs, the navigation of drug-loaded particles through the human vascular system under the action of magnetic fields was proposed by the researchers in the late 70s [1,2]. In this frame, the healthy cells remain unaffected by the drug and the side-effects are minimized. On the other hand, the therapeutic efficiency is optimized as a result of the increased quantities of drug that reach the tumour area [3].

Iron oxides (Fe<sub>3</sub>O<sub>4</sub>) have been investigated intensively for biomedical applications [4]. Iron oxide particles present many advantages such as low toxicity, high surface to volume ratio, magnetic properties and price [5]. In many cases magnetic nanoparticles are injected directly on the tumour when it is superficial but this is not feasible in other cases [6]. Thus, a way to navigate nanoparticles to the desired tumour is an issue in order to minimize the drug dose for the avoidance of side effects [7]. For this reason magnetic navigation

of nanoparticles with the use of appropriate external magnetic fields has been proposed, since the particles are used in Magnetic Resonance Imaging (*MRI*) and are visible with the use of it [8].

The magnetic navigation of particles depends on the type of nanoparticle material as well as the magnitude of the magnetic field [9–11]. However, as the flow velocity is decreased through the arteries, smaller magnitudes of the magnetic field are needed for an efficient magnetic driving of nanoparticles [12]. The size of magnetic nanoparticles (*MNPs*) is a crucial factor for the efficiency of the navigation [13,14]. The smaller the particles, the less they are magnetized and therefore they are not responding to the magnetic field [15–17]. Thus, it becomes apparent that a numerous parameters should be taken into account for the optimization of the performance of the magnetic targeted drug delivery [15–17] given the fact that the use of large particles could form clots in arteries and arterioles [18]. On the other hand, very small particles are carried away by the fluid, resulting in increased difficulty for particles to be driven into artery bifurcations [15].

In order to overcome these limitations, paramagnetic particles can be used, where, under the influence of a steady magnetic field, attract each other, resulting in aggregates which exhibit greater magnetization and hence increased magnetic response [13]. This occurs due to the greater magnetic moment of the agglomerates compared to the isolated particles. In the case of anticancer therapy, the agglomerates must be separated into isolated particles to deposit the drug into the cancer cells, upon reaching the desired area. Paramagnetic particles, lose their magnetization in the absence of the magnetic field so they can be easily separated in the absence of the magnetic field [19,20].

Materials that are affected by the magnetic field were also investigated for hyperthermia treatment of cancer [21]. A new therapeutic system called magnetic hyperthermia therapy (*MHT*) is already developed [22]. The *MHT* technique is based on heat that is generated by magnetic nanoparticles (*MNPs*) under the action of the alternating magnetic field. The results from *MHT* method are very promising, but a typical limitation of its usage is localizing heat solely to tumour areas sparing healthy surrounding tissues [23]. Under the combined action of a permanent magnetic field along with an alternating magnetic field, heating focus may be achieved to smaller regions in a tunable manner [24]. It is very important for the above applications to be able to accurately control the position and the trajectory of the particles in order to navigate them in specific areas while they are moving into a biological fluid e.g., in the cases of arteries [25] or inside scaffolds [26] and ligaments [27].

In recent years, there are numerous researchers that are trying to find ways in order to overcome the difficulties in the magnetic navigation of nanoparticles. The use of amplitude modulation magnetic particle imaging with soft magnetic core can shorten the necessary driving time by 25% while can improve the imaging resolution by 43% compared to the conventional methodology employed [28]. In addition, co-encapsulation of magnetic nanoparticles and anticancer drug into biodegradable microcarriers is suggested as a method to improve drug targeting in deep tissues [29]. Furthermore, a one dimensional nanoparticle navigation method can successfully manipulate and monitor the nanoparticles under 2 Hz navigation update rate with a field gradient of 3.5 T/m during the imaging mode and 8.75 T/m during the actuation mode in a tube [30]. Moreover, a nanorobotic platform that integrates many inter-disciplinary components and methods within physiological, technological constraints and tight real-time for operations in the blood vessels and microvasculature system is proposed in [31]. Additionally, a magnetic navigation method that drives a swarm of nanoparticles to an area that guarantees their successful guidance towards a desired direction using an asymmetrical field function to handle swarm of nanoparticles is introduced in [32]. Then, a transporter field function is used to transfer the particles between the desired areas, and finally a sustainer field function is used to keep the particles within the desired zone.

Although driving of magnetic nanoparticles is achieved in all the above applications, so far there is a lack of methodologies that succeed optimum guidance of nanoparticles.

For this reason, an optimization algorithm is used in this study for the first time in three dimensional arrays in order to control the magnetic field along with the computational model of particle motion in blood flows [15,33,34]. The optimization algorithm for determining and controlling the magnetic field that is used in the present study is the Covariance Matrix Adaptation Evolution Strategy (CMAES) [35]. The CMAES algorithm is used to navigate the particles to a targeted area through successful adjustments in the phase and magnitude of the magnetic gradient that can be imposed by MRI. The CMAES method is an evolutionary strategy based on the evolutionary calculation which is determined by a class of stochastic optimization methods. This optimization method has already been successfully tested for removing particles from two-dimensional simplified Y-shaped branch geometries [12].

In the present study, a computational method for optimal magnetic navigation of nanoparticles inside human arteries is presented. The numerical methodology for the kinetics and the navigation of nanoparticles into the desired areas as well as simulation details are presented in Section 2. Results from the simulations are presented and discussed in Sections 3 and 4, respectively. Finally, conclusions are summarized in Section 5.

## 2. Materials and Methods

### 2.1. Governing Equations

In this study a numerical procedure for the evaluation of the optimal gradient magnetic fields for the navigation of magnetic nanoparticles inside a carotid artery is presented. For the propulsion model of the particles seven major forces are considered, i.e., the magnetic forces from MRI's main magnet static field as well as the Magnetic field gradient force from the special propulsion gradient coils. Moreover, the contact forces among the nanoparticles and the carotid walls, and the Stokes drag force for each particle are considered. In addition, gravitational forces and the force due to buoyancy are included. Finally, Van der Walls force and Brownian motion are taken into consideration in the simulation. Flow field and the uncoupled equations of particles motion are calculated using the OpenFOAM platform [36]. Laminar blood flow is expected to occur in the carotid model. The incompressible Navier–Stokes equations are solved for the Eulerian frame along with a model for the discrete motion of particles in a Lagrangian frame. The governing equations of the fluid phase are given as following:

$$\nabla \cdot u = 0 \quad (1)$$

$$\frac{\partial u}{\partial t} + u \cdot \nabla u = -\frac{\nabla p}{\rho} + \nu \nabla^2 u \quad (2)$$

where  $t$  is the time,  $u$  and  $p$  are the fluid velocity and pressure, respectively, and  $\rho$  and  $\nu$  are its density and kinematic viscosity, respectively. In this study, blood is considered as a non-Newtonian fluid. Therefore, the Bird-Carreau model is adopted in this study, where the viscosity of the blood is given by the following equation [37]:

$$\nu = \nu_{\infty} + (\nu_0 - \nu_{\infty})[1 + \lambda^2 \dot{\gamma}^2]^{\frac{(n-1)}{2}} \quad (3)$$

where,  $\dot{\gamma}$  is the shear rate,  $\nu_{\infty}$  is the viscosity at infinite shear rate,  $\nu_0$  is the viscosity at zero shear rate,  $\lambda$  is relaxation time and  $n$  is the power index power.

The equations of every particle single motion in the discrete phase are based on the Newton law and may read as follows:

$$m_i \frac{\partial u_i}{\partial t} = F_{mag,i} + F_{nc,i} + F_{tc,i} + F_{drag,i} + F_{grav,i} + F_{wvdv,i} + F_{br,i} \quad (4)$$

$$I_i \frac{\partial \omega_i}{\partial t} = M_{drag,i} + M_{con,i} + T_{mag,i} \quad (5)$$

where, the index  $i$  stands for the  $i$ th-particle with diameter and mass noted by  $d_i$  and  $m_i$ , respectively.  $I_i$  is the mass moment of inertia matrix while  $t$  is time and  $u_i$ ,  $\omega_i$  are its transversal and rotational velocities, respectively. Terms  $\frac{\partial u_i}{\partial t}$  and  $\frac{\partial \omega_i}{\partial t}$  correspond to its linear and angular accelerations, respectively.  $F_{mag,i}$  is the total magnetic force, while  $F_{nc,i}$  and  $F_{tc,i}$  stands for the normal and tangential contact forces, respectively,  $F_{drag,i}$  and  $F_{grav,i}$  are the hydrodynamic drag and buoyancy forces, respectively, and  $F_{wv,i}$  and  $F_{br,i}$  are the Van der Waals and Brownian forces, respectively.  $M_{drag,i}$  and  $M_{con,i}$  are drag and contact moments, respectively, and finally,  $T_{mag,i}$  is the magnetic torque at the position of particle  $i$ . All forces and moments are calculated according to Discrete Element Method (DEM) method as in [15]. Details of the numerical models, forces and moments terms used on particles are given in [15–17].

For the evaluation of the potential of the computational platform a carotid model is studied here, as depicted in Figure 1. The dimensions of a human carotid model are described in Ref. [38]. For the establishment of fully developed velocities profiles before the bifurcation and in order to diminish the numerical issues which are connected to the boundary conditions, the computational geometry is suitably expanded in the inlet and outlets. For this reason, the overall length of the carotid geometry model is 0.3 m. The 3D computational mesh is developed using the Gmsh mesh generator [39]. Representative views of the computational unstructured mesh, at the inlet and the bifurcation of the carotids, are presented in Figure 2.

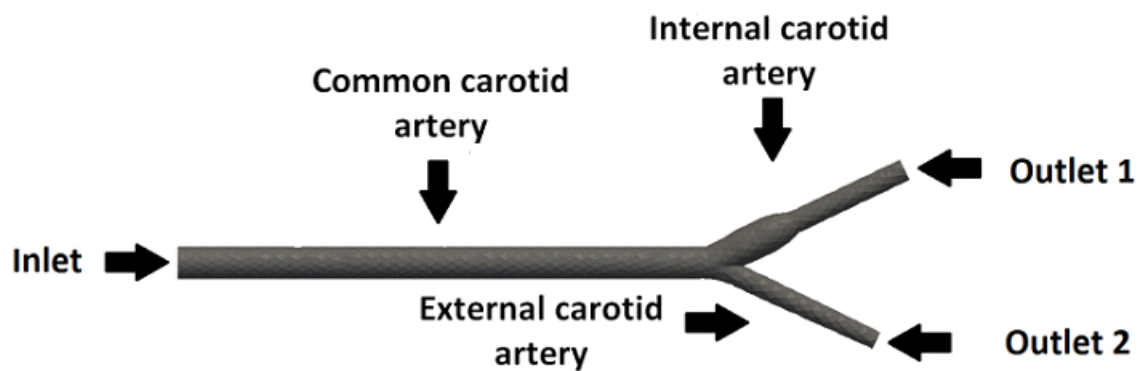


Figure 1. Carotid geometry.

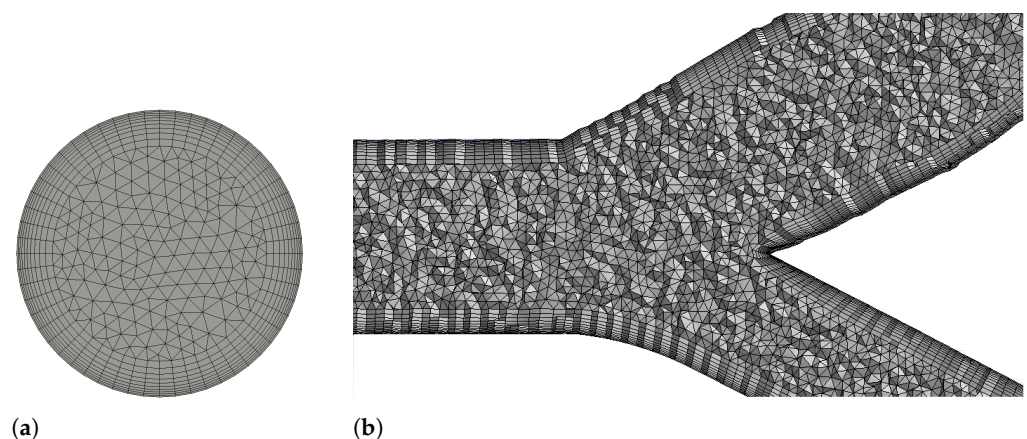


Figure 2. Computational mesh at the (a) inlet, and (b) inside of the carotid bifurcation.

## 2.2. Model Validation

The numerical model for the motion of particles that is employed in this study has already been successfully validated in [15–17]. The motion of blood inside human arteries is validated against the experimental results of [40]. The developed carotid model imposed

in the same blood flow conditions as in [40]. In addition, the evaluation of the flow is measured six diameters upstream the apex of the bifurcation. The values of each parameter of the Bird-Carreau model that were used in the simulations are presented in Table 1. The axial blood flow for both experimental measurements of [40] and the results of the current simulation are presented in Figure 3. It is observed that the results show good qualitative agreement. A difference of only 3% is encountered between experimental data of [40] and the present numerical model.

**Table 1.** Simulation parameters.

Bird-Carreau Parameters		
Symbol	Value	Unit
$\nu_{\infty}$	$2.2 \times 10^{-3}$	Pa·s
$\nu_0$	$22 \times 10^{-3}$	Pa·s
$\lambda$	0.11	s
$n$	0.392	-

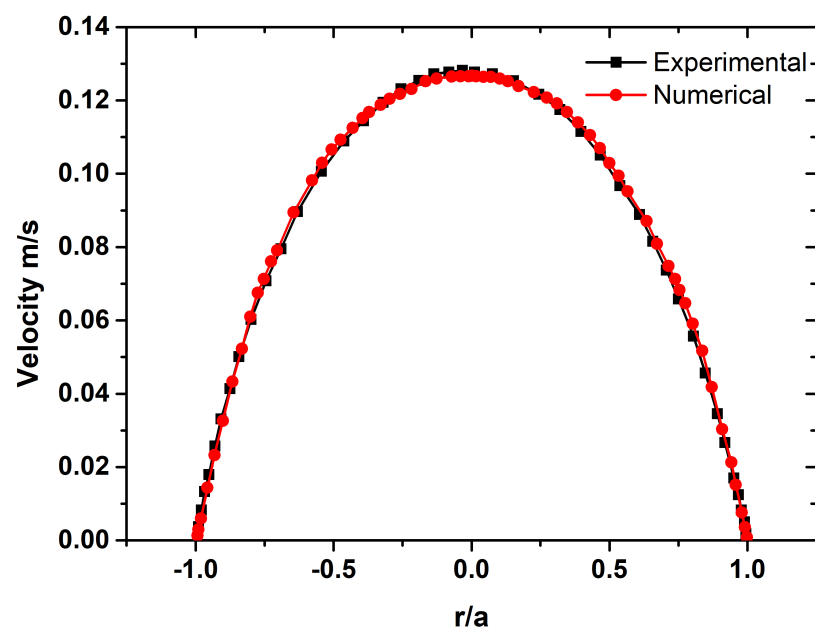


**Figure 3.** Comparison of axial blood velocity between experimental measurements (black) of Ref [40] and present numerical simulation (red).

### 2.3. Determination of the Appropriate Magnetic Gradients

The CMA evolution strategy algorithm [35] is used along with CFD and DEM software in order to navigate the particles into a desired path through successive variations of the magnetic gradient magnitude and sign. The CMA algorithm conducts an iterative principal component analysis of successful search steps, while retaining all principal axes. In addition, two paths of the time evolution of the mean distribution are recorded, called search or evolution paths, respectively. These paths include significant information about the correlation between consecutive steps. In particular a gradient magnetic field is selected by sampling a multi-variate normal distribution.

The basic equation for sampling the magnitudes of the gradient magnetic field, for generation number  $g = 0, 1, 2, \dots$  is

$$\mathbf{x}_k^{(g+1)} \sim \left( \mathbf{m}^{(g)}, (\sigma^{(g)})^2 \mathbf{C}^{(g)} \right) \text{ for } k = 1, \dots, \lambda \tag{6}$$

where  $\sim$  indicates the same distribution on left and the right side,  $\mathbf{x}_k^{(g+1)} \in \mathbf{R}^n$ ,  $k$ -th offspring (search point) from generation  $g + 1$ ,  $\mathbf{m}^{(g)} \in \mathbf{R}^n$ , mean value of the search distribution at generation  $g$ ,  $\sigma^{(g)} \in \mathbf{R}_+$ , overall standard deviation, step size, at generation  $g$ ,  $\mathbf{C}^{(g)} \in \mathbf{R}^{n \times n}$ , covariance matrix at generation  $g$ , and  $\lambda \geq 2$ , population size, sample size, number of offspring.

The new mean of the search distribution is calculated by :

$$\mathbf{m}^{(g+1)} = \sum_{i=1}^{\mu} w_i \mathbf{x}_{i:\lambda}^{(g+1)} \tag{7}$$

$$\sum_{i=1}^{\mu} w_i = 1 \quad w_i > 0 \text{ for } i = 1, \dots, \mu \tag{8}$$

where  $\mu \leq \lambda$  is the parent population size, i.e., the number of the variations of the gradient magnetic field in each simulation.  $w_i = 1 \dots \mu \in \mathbf{R}_+$ , positive weight coefficients for recombination, where  $w_1 \geq w_2 \geq \dots \geq w_{\mu} > 0$ .  $\mathbf{x}_{i:\lambda}^{(g+1)}$ ,  $i$ -th the best individual out of  $\mathbf{x}_1^{(g+1)}, \dots, \mathbf{x}_{\lambda}^{(g+1)}$  from Equation (6). Finally, the covariance matrix at generation  $g + 1$  is given by:

$$\mathbf{C}^{(g+1)} = \sum_{i=1}^{\mu} w_i \left( \mathbf{x}_{i:\lambda}^{(g+1)} - \mathbf{m}^g \right) \left( \mathbf{x}_{i:\lambda}^{(g+1)} - \mathbf{m}^g \right)^T \tag{9}$$

#### 2.4. Driving Process

In this work, the above mentioned method is used for the first time in the navigation of paramagnetic nanoparticles in three-dimensional geometries. It should be noted that the present method was successfully employed in two-dimensional navigation problems [12]. The method intends to minimize the particles position deviation from a desired path. The desired trajectory in all simulations is preset and described in the computational method by a 10 degree polynomial as is depicted in Figure 4.

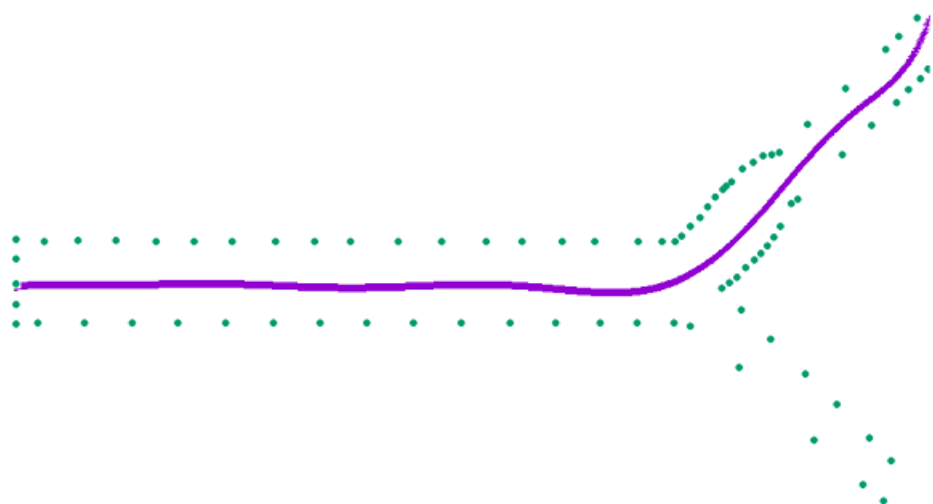


**Figure 4.** Projection of the carotid artery. Desired trajectory (purple line) and walls (green dots).

Initially, blood flow in the carotid is achieved by suitably solving Equations (1) and (2). The non-Newtonian nature of blood’s viscosity is taken into consideration by solving Equation (3). Upon solving the flow and the pressure fields, the discrete phase simulation (DEM) starts by solving Equations (4) and (5). Blood loaded with particles enters the carotid from the left and splits into the two outlet branches at the right side of the domain (Figure 1). Random

magnitudes of the gradient magnetic field are provided from *CMA* evolution strategy to *DEM* in the beginning of the process as an initial guess. The *DEM* method evolves all particles' positions for some time and the deviation between the nanoparticles and the desired trajectory is evaluated in each time step. The discrete phase simulation starts with combination of the *DEM* and the *CMA* methods. The *CMA* algorithm is used in order to minimize the deviation from the desired trajectory by providing more appropriate magnitudes of the gradient magnetic field in each simulation by solving Equations (6)–(9). Hence, the optimal magnitudes of the gradient magnetic field are evaluated for optimum navigation of nanoparticles into the desired area. Representative duration of the numerical simulation under 18 variations of the gradient magnetic field is 24 and 120 h of CPU (Intel Xenon E5-2620 v3) time for 1 and 1000 simulated particles, respectively.

### 2.5. Simulation Details

A mesh dependency test using the boundary conditions of Table 2 is conducted in the carotid model, with 0.25, 0.75, 1.5 and 2 million cells. Results indicate that the difference in the computed velocity of outlet 1 between the cases of 1.5 and 2 million cells become practically zero, as is shown in Figure 5. Therefore, all simulations in this study are conducted in a carotid model with 1.5 million cells. The computational mesh is consisted of approximately 1.5 million tetrahedra and wedge elements. The latter are used at the vicinity of the walls to resolve the viscous boundary layers.

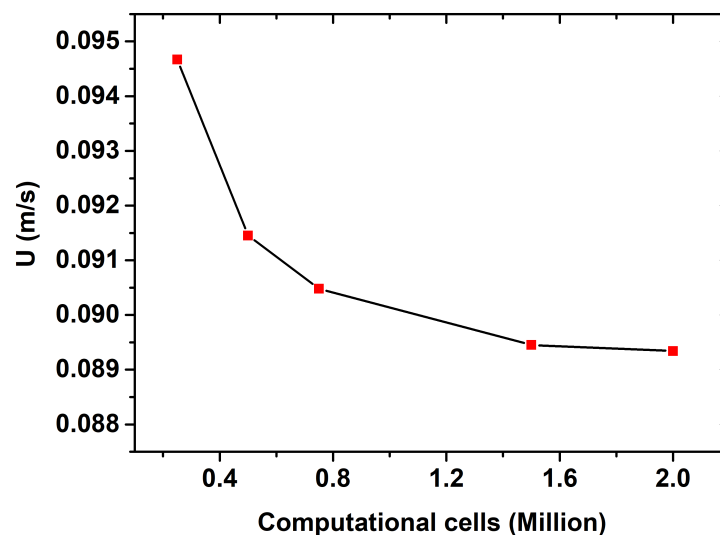


**Figure 5.** Velocity in the outlet 1 of the carotid model under different number of computational cells.

In this study, particles with sizes in the range 200 to 900 nm are placed in different locations in the inlet of the carotid model for the evaluation of the computational method. In addition, simulations with up to three thousand  $\text{Fe}_3\text{O}_4$  spherical particles are performed in this study. Furthermore, different concentrations of particles are used in order to evaluate the effect of the concentration in the magnetic navigation process. The physical material properties of particles and other important parameters used in this study are the same as in Ref. [17] and are summarized in Table 3. The boundary conditions that were used for the evaluation of the fluid flow in all the simulations are tabulated in Table 2.

In the present study, we intend to navigate the nanoparticles under the combined action of permanent and gradient magnetic fields from the common to the internal carotid artery (Figure 1). Therefore, the desired trajectory (Figure 4) is successfully transformed into a 10 degree polynomial and imported in the computational platform. It should be noted that the steady magnetic field is set equal to  $B_0 = 10 \text{ T}$  in all simulations while the magnetic gradient is constantly changing in order to drive the nanoparticles as close in the desired path [41]. In this study, the range of the permitted gradient magnetic field magnitude is

set to  $\pm 10$  T/m. Therefore, only magnitudes in the above mentioned range are generated by the CMA evolution strategy. In addition, the magnetic gradient is changing 18 times in each simulation. Furthermore, each iteration of the computational method includes 10,000 evaluations of the gradient magnetic field values. At the start of each simulation, the nanoparticles are randomly distributed and placed just after the inlet boundary. It should be noticed that the computational method is evaluated under the most difficult conditions since the nanoparticles are placed in the opposite direction of the carotid brach that intended to be navigated and just above the walls of the carotid.

**Table 2.** Boundary conditions.

Boundary Conditions		
Boundary	Velocity	Pressure
Inlet	0.08 m/s	Zero gradient
Outlet 1	Zero gradient	0
Outlet 2	Zero gradient	0
Walls	0	Zero gradient

**Table 3.** Particles' and simulations conditions.

Property	Units
Particles' density	5000 Kg/m <sup>3</sup>
Young's modulus	$3.5 \times 10^9$ Pa
Poisson's ratio	0.34
Relative magnetic permeability	1.23
Medium permeability	$1.256 \times 10^{-6}$
Temperature	288 K
Molecular mean free path	$2.5 \times 10^{-9}$

### 3. Results

In this study, the computational platform is used in order to navigate the nanoparticles from the common to the internal carotid artery through a desired trajectory (Figures 1 and 4). The diameter of the particles is a crucial parameter for an effective magnetic navigation [15]. The magnetic moment of each particle is affected by its volume. Therefore, particles with small diameters are very difficult to be navigated towards the desired locations. This effect is presented in Figure 6 where the particles with diameter of 200 nm are not navigated into the desired branch of the carotid Figure 6a. It should be noted that the computational platform under the permitted limits of the imposed gradient magnetic fields are not able to successfully navigate the particles into the desired branch of the carotid. On the other hand, under the same magnetic gradient limits and under the appropriate gradient magnetic field adjustments the particles with diameter of 500 nm follow as close as possible the desired trajectory, as is depicted in Figure 6b.

Results of the present study indicate that particles with diameter from 200 to 400 nm under the imposed gradient limits are unable to be driven into the desired location. This effect is presented in Figure 7. On the other hand, the computational platform can successfully drive particles with diameter above 500 nm, as is depicted in Figure 7. It should be noticed that bigger particles are moving towards the common carotid in less time although the blood velocity is the same among the simulations, as is depicted in Figure 7. This effect is caused due to the easier manipulation of the bigger particles by the magnetic field. Therefore, the bigger particles are moving towards the common artery in areas with increased flow velocity. The closer (best), average and worst distances of particles from the desired trajectory in the whole simulation and in each iteration of the computational model for the whole range of the simulated diameters are presented in Figure 8. The gradient magnetic field values are evaluated in terms of the closer distance of nanoparticles

from the desired trajectory. The average and worst distances of nanoparticles from the desired trajectory indicate the way that the computational platform evaluate the appropriate gradient magnetic field values. In this study, the distance of particles from the desired trajectory in the whole simulation is defined as the sum of the mean distance of particles from the desired trajectory in each change of the gradient magnetic field in the simulation. In this way, the search distribution of the appropriate gradient magnetic field magnitudes is minimized. Therefore, less time is needed for the selection of the optimum values by the computational method.

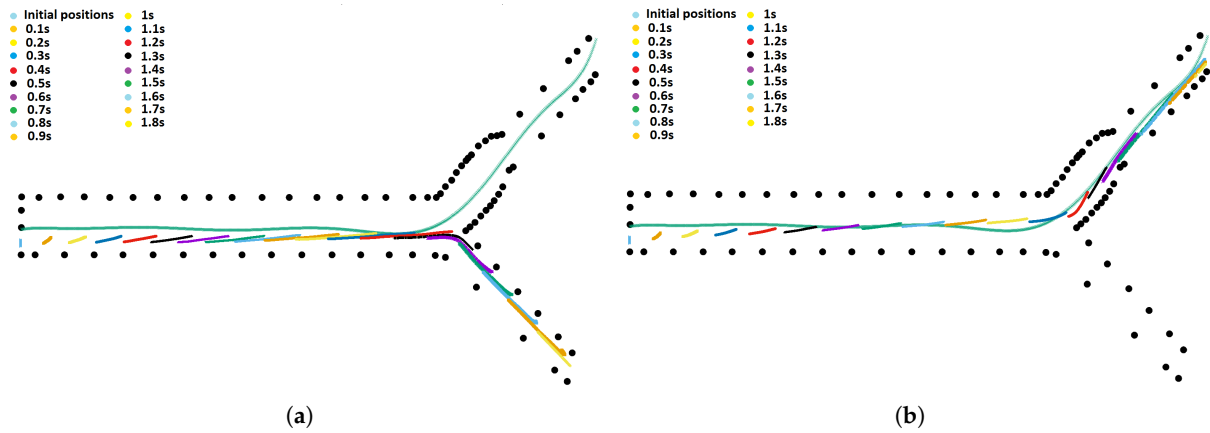


**Figure 6.** Projection of the positions of particles under different time steps of the navigation process for particles with diameter of (a) 200 nm and (b) 500 nm. Desired trajectory (cyan line) and walls (black dots).

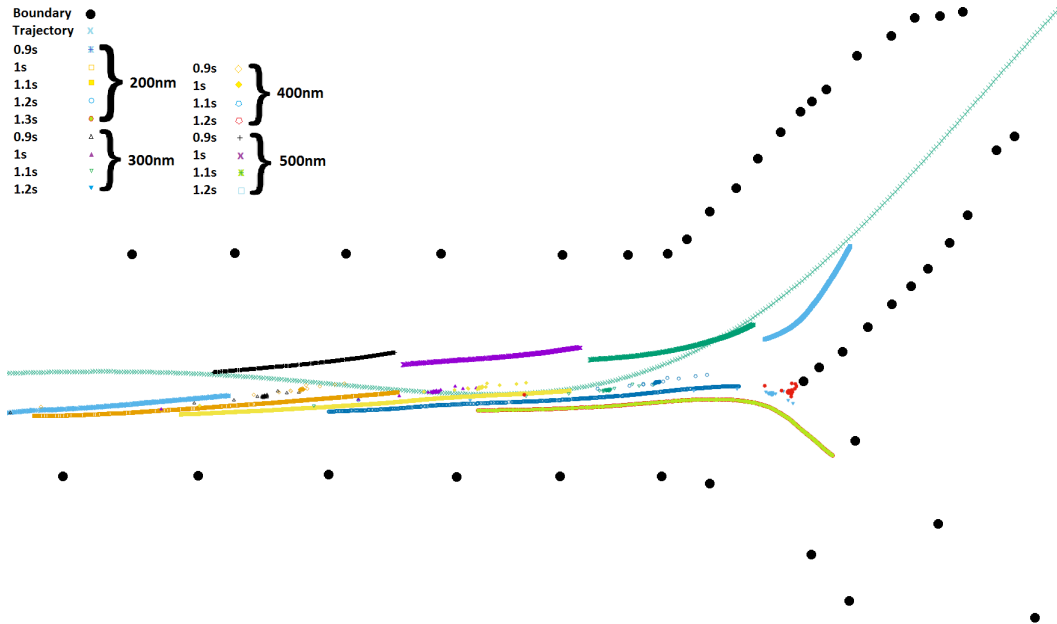


**Figure 7.** Projection of the positions of different diameter particles under different time steps of the navigation process.

The computational platform perform validation of the gradient magnetic field values and select the best of them for optimum magnetic navigation of particles, as it is depicted in Figure 8a,b. It should be pointed out that the evolution of the simulation process leads to closer distances of particles from the desired trajectory in each iteration. Since its iteration is composed by 10,000 different evaluations of the gradient magnetic field values, the evolution of average and worst distances of the particles from the desired trajectory is presented in Figure 8c–f, respectively. It should be noticed that only the gradient magnetic

field values of the best simulation are used from the computational algorithm for the generation by the *CMAES* of the values of the gradient magnetic field for the next iteration. Consequently, the values of the simulation with average and worst distances from the trajectory are not adopted by the computational platform for the next iteration step.

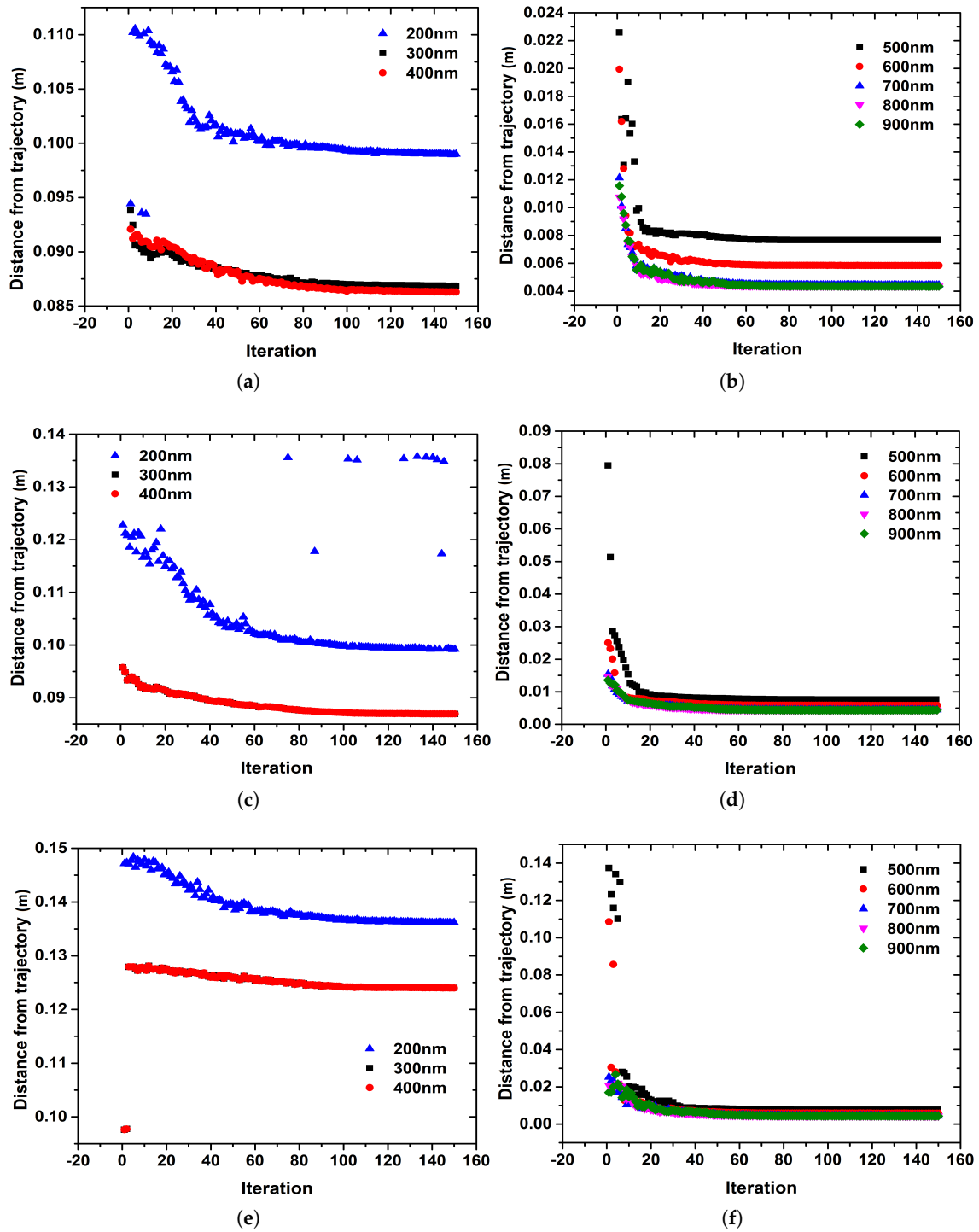


Figure 8. (a,b) Best, (c,d) Average and (e,f) Worst distance of particles in each iteration from the desired trajectory.

The diameter of particles has a serious impact in the computational time that is needed for the computational algorithm to evaluate the gradient magnetic field for optimum navigation. For particles with diameter from 200–400 nm the optimum values of the gradient magnetic field are evaluated approximately after 110 iterations, as it is depicted in Figure 8a. On the other hand, in the simulations with particles of 500–900 nm, only 60 iterations are required for obtaining the gradient magnetic values for optimum navigation inside the carotid, as it is depicted in Figure 8b.

The diameter of particles plays a significant role in the magnetic navigation process since in the diameter range of 200–400 nm, the gradient magnetic field (T/m) is not sufficient enough in order to navigate the particles in the desired branch of the carotid and close to the trajectory (Figure 8a) and therefore the distances from the trajectory are higher than that of particles in the range of 500–900 nm (Figure 8b). This effect in terms of percentage difference ( $\Delta I$ ) between the case of 400 and 900 nm is presented in Figure 9. It should be noted that an increase of 44% in the diameter of the nanoparticles leads 96% closer the nanoparticles to the desired trajectory. It should be noticed that even from the first iterations larger nanoparticles (900 nm) can be navigated 88% closer to the desired trajectory. As the evaluation of the gradient magnetic fields continues, this difference become equal to 96%, as is depicted in Figure 9. For example, after five iterations the computational platform manage to navigate the particles with diameter of 900 nm approximately 91% closer to the desired trajectory compared to the simulation with particles of 400 nm. This difference is minimized and remains steady after approximately 90 iterations of the computational platform. Finally, the particles of 900 nm are navigated 96% closer to the desired trajectory compared to the particles of 400 nm, as is depicted in Figure 9.

Based on the predefined gradient magnetic limits, only particles with diameter of 500 nm and above can effectively be navigated close to the trajectory and into the desired areas by the computational platform. Therefore, the percentage difference of the best values of the gradient magnetic field from the case of 500 nm in each change of the gradient magnetic field in each simulation is presented in Figure 10a. As the diameter of particles increases, the values of the gradient magnetic field that are evaluated by the computational method for optimum navigation of particles into the desired trajectory are decreased, as is depicted in Figure 10a. It should be pointed out that the same values of the gradient magnetic field are evaluated by the computational method during the simulations. For example, there is no difference in the imposed gradient magnetic field in changes 4, 10, 11 and 12, as is depicted in Figure 10a.

The overall difference in the values of the gradient magnetic field from the case of 500 nm is presented in Figure 10b. As the diameter of particles is increased an exponential decrease in the difference from the case of 500 nm of the appropriate values of the gradient magnetic field that are needed for optimum navigation is observed. Approximately 35% lower values of the gradient magnetic field are needed for an effective navigation of particles in the desired areas in the case of 600 nm. This difference is maximized in the case of 900 nm where 71% smaller values of the gradient magnetic field are used compared to the case of 500 nm for optimum navigation into the desired areas as is depicted in Figure 10b.

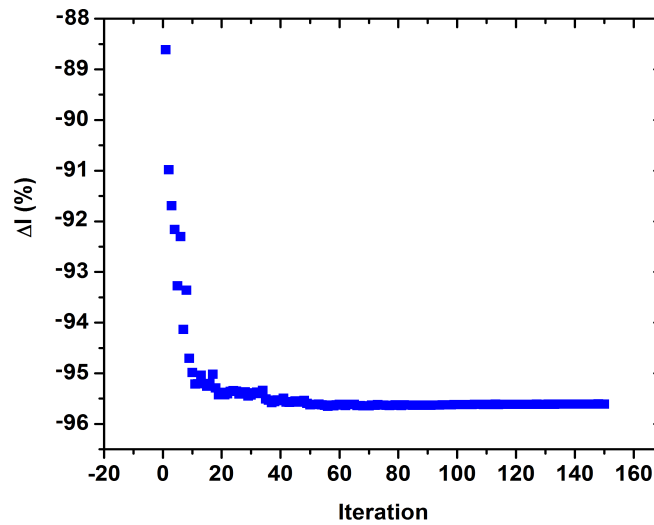


Figure 9. Percentage difference from desired trajectory between the cases of 400 and 900 nm.

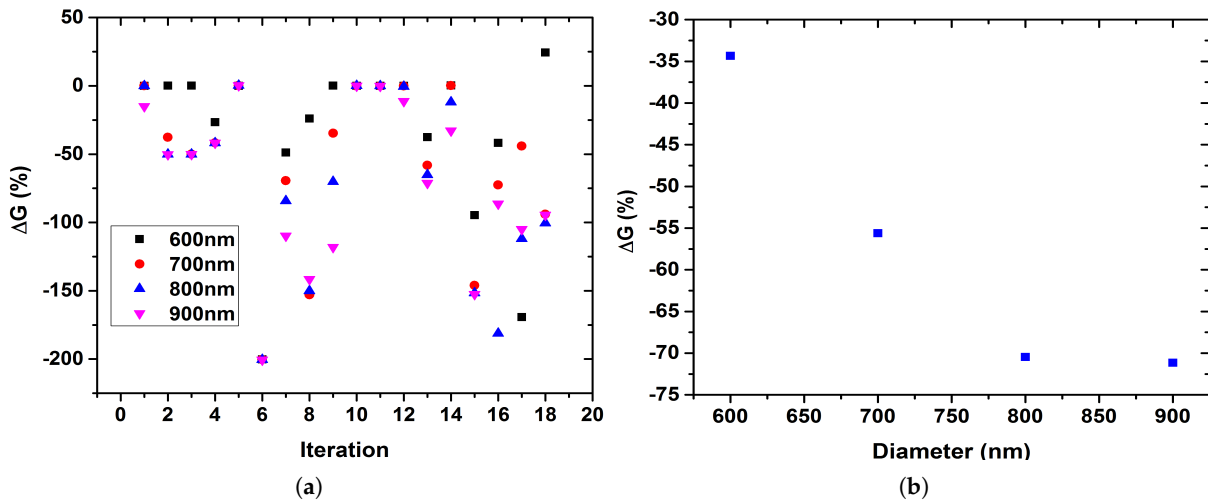


Figure 10. (a) Gradient magnetic field change from the case of 500 nm, (b) Overall percentage difference from the base case of 500 nm.

In order to examine the potential of the magnetic navigation method, the exact same simulations are performed with 25% reduction in the inlet velocity. The closer distance of particles from the desired trajectory in each iteration and for all the range of the simulated particles is depicted in Figure 11. It should be noticed that nearly the same trend in the driving process of the particles as in Figure 8a,b is observed. Therefore, the velocity of the blood seems to have insignificant effect in the evaluation process of the appropriate magnitudes of gradient magnetic field that is performed by the computational method. On the other hand, it should be pointed out that at the end of the navigation process the particles are approximately 3% closer to the desired trajectory in the simulation with smaller inlet velocity, as is depicted in Figure 12.

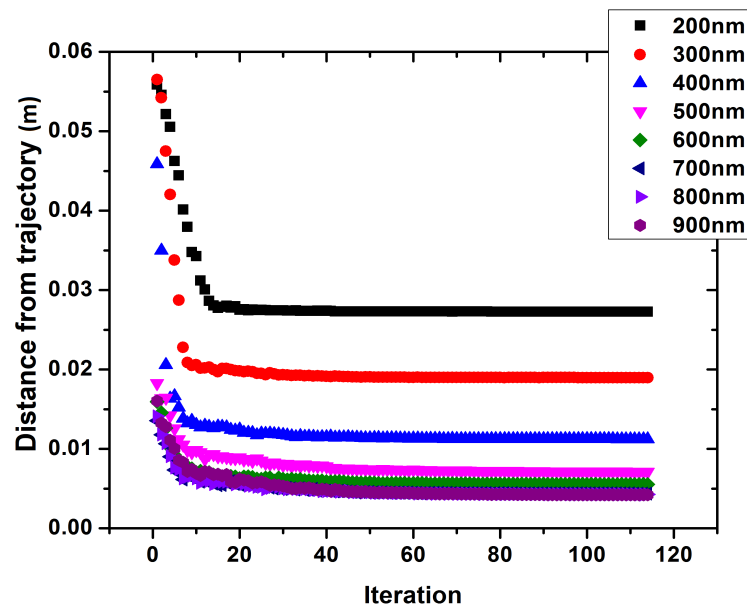


Figure 11. Distance of particles from the desired trajectory in each iteration of the computational method under inlet velocity of 0.06 m/s.

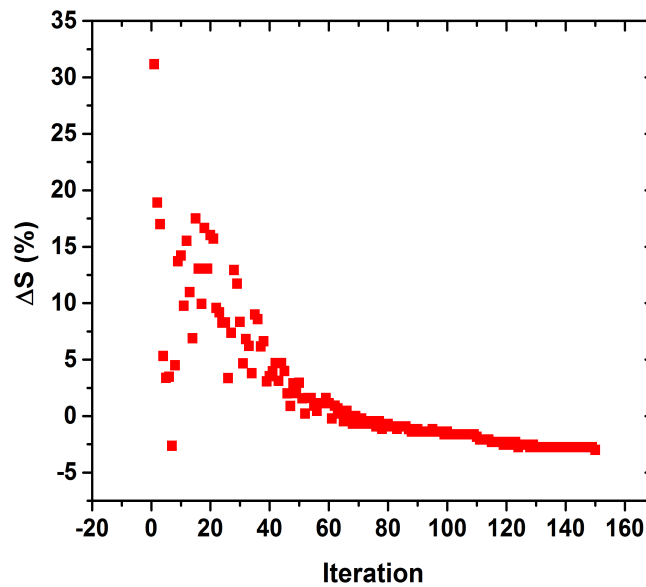
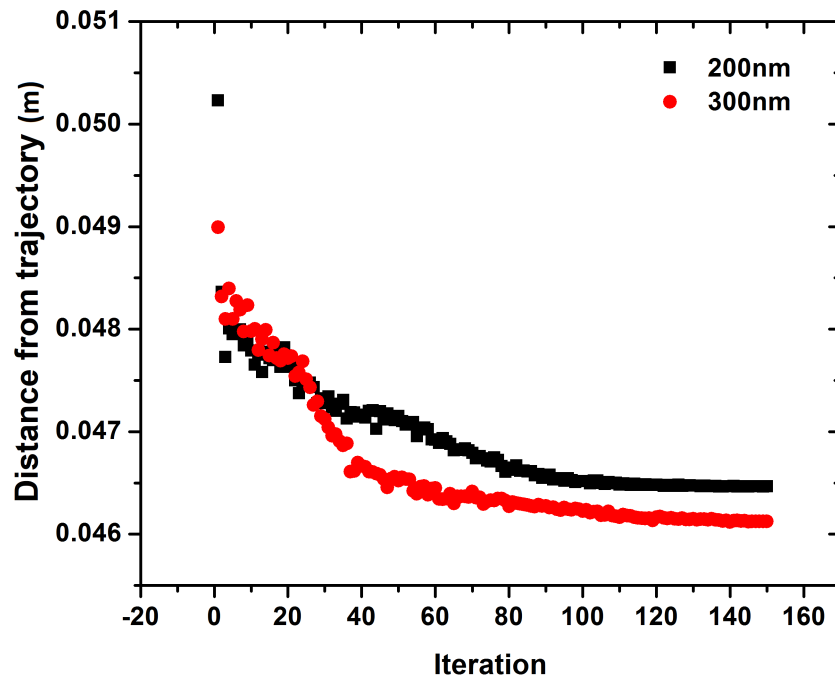


Figure 12. Percentage difference of distance of particles ( $\Delta I$ ) with diameter of 800 nm from the desired trajectory between inlet velocity 0.08 m/s and 0.06 m/s.

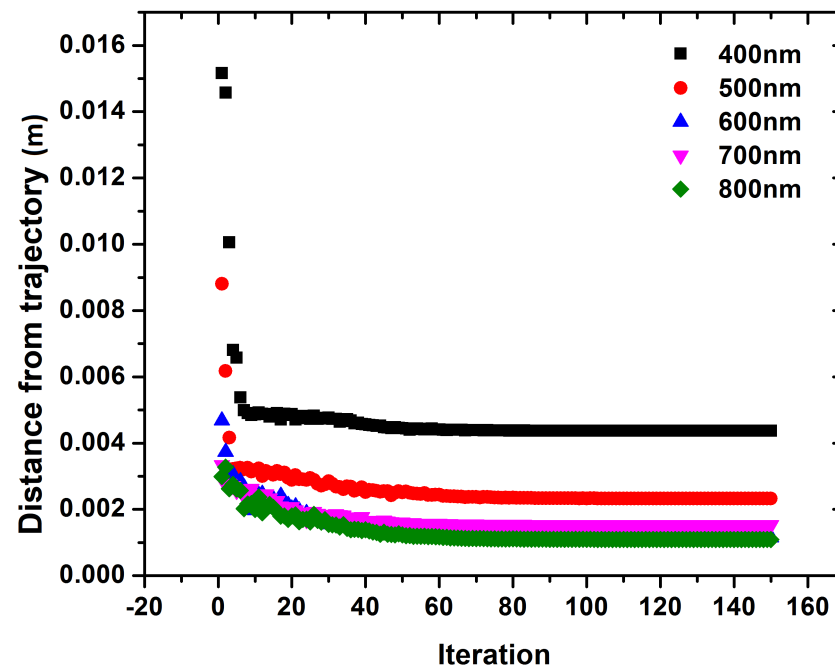
The effect of the diameter of the artery system in the magnetic navigation process is also studied in this study. For this reason, under inlet velocity of 0.08 m/s the diameter of the carotid artery is reduced by 50%. The closer distance of particles from the desired trajectory in each iteration and for all the range of the simulated particles is depicted in Figure 13. It should be noted that the profile of the evolution of the distance of particles from the desired trajectory is different in particles with smaller diameter than 300 nm (Figure 13a) compared to the other cases (Figure 13b). As the diameter of particles is increased the evolution profile follow the same trend as in the corresponding cases of Figure 8.

The diameter of the artery system has a crucial effect in the effectiveness of the magnetic navigation method. Although the diameter of the carotid artery is minimized by 50% the computational method manage to navigate the particles by 75% closer to the desired

trajectory compared to the corresponding cases of Figure 8, as is depicted in Figure 14. The difference in the distance of particles in each iteration of the computational method between the minimized artery and the carotid artery of Figure 1 for the representative case of particles with diameter of 800 nm is depicted in Figure 14.



(a)



(b)

Figure 13. Distance of particles from the desired trajectory in each iteration of the computational method under inlet velocity of 0.08 m/s in the minimized carotid artery for the cases of (a) 200, 300 nm, and (b) 400 nm and above.

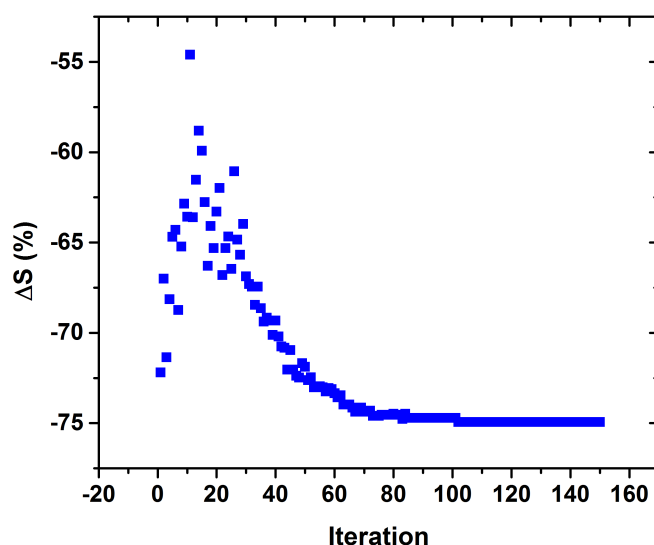


**Figure 14.** Percentage difference of distance of particles with diameter of 800 nm from the desired trajectory between the original and the minimized carotid artery under inlet velocity of 0.08 m/s.

#### 4. Discussion

In this study a new computational method for optimal magnetic navigation of nanoparticles inside the human vascular system is presented. It should be noticed that the blood velocity fields that are used in this study is only for demonstration purposes for the functionality of the method. The velocity of blood in the main arteries of the human vascular system such as aorta and neck arteries is higher than the velocities that are used in this study [42,43]. On the other hand, the blood velocity in arterioles is lower compared to the blood velocities of the present study [44].

Results indicate that the diameter of particles is the most significant parameter for the navigation into the desired locations. An increase in the diameter of the particles leads to an increase in the magnetic volume of particles [13–15]. Therefore, bigger particles are easier driven by the gradient magnetic field. It should be noticed that the easier manipulation of the bigger particles can lead in differences in the navigation process since the particles can be navigated in areas with high and lower flow velocities easier. The computational method that is developed in this study, can evaluate the appropriate gradient magnetic field values for optimum navigation of particles into the desired areas. The method that is proposed here can drive approximately 99% of the nanoparticles close to the desired trajectory. Consequently, the majority of the simulated particles are navigated as close as possible to the predefined target. It seems that the constant changes in the phase and the magnitude of the magnetic field is more efficient way to navigate particles in the desired areas compared to a steady gradient magnetic field [29]. It should be noticed that even with the worst values that have occurred after the evaluation of the computational method the nanoparticles can be navigated into the desired branch of the carotid but not close to the desired trajectory. It should be noticed that using the present method the particles that are coated with the anticancer drug are moving close to the desired trajectory and not close to the walls of the arteries as in [45]. This is very crucial since the particles moving near the wall may be trapped [46].

Only nanoparticles with diameter greater than 500 nm can successfully be navigated into the desired branch of the carotid. Smaller particles cannot be driven by the imposed magnetic field due to their small magnetic volume [14]. Therefore, the particles are moving away from the desired trajectory and are located in different than the desired branch of the carotid artery. This is caused due to the predefined limits in the range of the values of the gradient magnetic field. It should be pointed out that smaller nanoparticles can be

successfully navigated into the desired locations by increasing the range of values of the gradient magnetic field [15].

The increase of the diameter of particles not only increases the efficiency in the magnetic navigation process but also decreases the necessary gradient magnetic field values for an efficient navigation [12]. An increase of 44% in the diameter of the nanoparticles leads 96% of the nanoparticles closer to the desired trajectory. It should be noted that by increasing the diameter of the particles a reduction up to 200% in the magnitude of the gradient magnetic field for efficient driving is achieved. The mean reduction of the magnitude of the gradient magnetic field in each simulation compared to the case of 500 nm is from 35–71% with the increase of the diameter of particles. This effect is due to easier manipulation of bigger particles by the magnetic field due to the increased volume [13]. Therefore, lower magnitudes of the gradient magnetic field are evaluated by the computational method.

Although the increase of the diameter of particles leads to smaller magnitudes of the gradient magnetic field for an efficient navigation, there are times in the navigation process that both small and big particles are imposed under the same values of the gradient magnetic field. This effect is caused due to the deviation of the particles from the desired trajectory. As both small and big particles are away from the trajectory, the *CMAES* evaluate the maximum magnitudes of the gradient magnetic field in order to navigate the particles closer to the trajectory [35]. It should be noticed that higher values are needed sometimes in the cases with bigger particles in order to manipulate the particles and navigate them as close as possible to the desired trajectory, especially after a bifurcation. This is due to the increased momentum of the bigger particles compared to smaller ones. In addition a crucial parameter for the imposed values is the geometry which the particles are navigated. A greater amount of changes in the gradient magnetic field is needed in complicated geometries such as the vascular system of the human due to the increased branching [12].

The decrease of the velocity seems to have an insignificant effect in the navigation of particles. Based on the imposed magnetic gradient limits the computational scheme allows the navigation of the particles closer to the desired trajectory with smaller blood velocity. An 25% reduction of the inlet velocity leads the particles only 3% closer to the desired trajectory. Therefore, the velocity of blood under the predefined range of the gradient magnetic field seems to play insignificant role in the magnetic navigation of particles by the computational method. On the other hand, the reduction of the inlet velocity has a crucial effect on the time of the evaluation of best values of the gradient magnetic field for optimum magnetic navigation. Based on the results, approximately 10 iterations less, from the total of 150, are needed for particles with diameter above 500 nm for the evaluation of the best gradient magnetic field values compared to the cases with inlet velocity 0.08 m/s. For particles with diameter below 500 nm the evaluation of the appropriate gradient magnetic field values require 20–35 iterations of the computational method. This is a huge difference compared to the case with inlet velocity 0.08 m/s which approximately 110 iterations are required. This effect is caused due to the enhanced searching of values by the *CMAES* [35]. Under lower velocities of blood, the differences in the distance of particles from the desired trajectory are minimized among the iterations at an increasing rate compared to the cases with increased velocity.

The results of the computational method indicate that the smaller the diameter of the artery system, the higher the effectiveness of the magnetic navigation method. As the diameter of the arteries are decreased the particles are navigated closer to the desired trajectory. It should be noticed that the decrease in the distance of particles from the desired trajectory is not proportional to the reduction in the diameter of the artery system. Consequently, the present computational method is more efficient in the navigation of particles as the diameter of them is decreased. This is very significant since as is observed in experiment in pigs increased difficulty is observed in the manipulation of particles as the diameter of arteries is minimized [47].

## 5. Conclusions

The present model can simulate the motion of particles when they are navigated by the gradient magnetic field inside the human vascular. Under the influence of the blood flow, the model evaluates the effect of different values of the gradient magnetic field in order to minimize the distance of particles from the desired trajectory. The diameter of particles is a crucial parameter for an effective magnetic navigation. Small nanoparticles cannot be efficiently navigated by the computational method. Nanoparticles with diameter above 500 nm can be navigated into the desired trajectory with an efficiency of approximately 99%. Therefore, for an efficient navigation of small particles the magnitudes of the permanent and gradient magnetic field should be increased. The velocity of the blood seems to play insignificant role in the navigation process under the imposed range of the gradient magnetic field and changes in each simulation. A reduction of 25% in the inlet velocity leads the particles only 3% closer to the desired trajectory. Finally, the computational method is more efficient as the diameter of the vascular system is minimized. Under a reduction of 50% in the diameter of the carotid artery the computational method navigates the particles approximately 75% closer to the desired trajectory.

To the best of the authors' knowledge this is the first numerical model for optimization of the navigation of nanoparticles into the desired areas under the combined action of the permanent and gradient magnetic field. The proposed method can be used with increased efficiency in small arteries, arterioles and blood flows. In addition it can be used as a tool for the determination of the parameters that mostly affect the magnetic navigation of particles. Finally, it can assist in the quantification of the magnetic field magnitudes that are required for effective magnetic navigation in in-vivo and in-vitro experiments. In the near future, the effect of the components of blood in the magnetic navigation of nanoparticles will be investigated by the addition of the red blood cells in the computational model. Furthermore, the differences in the diameter of the blood vessels upon the cardiac cycle will be taken into consideration by enabling the uncertainty quantification method into the present model.

**Author Contributions:** Conceptualization, E.K. and T.K.; methodology, E.K.; software, A.T.; validation, E.K., C.L.; formal analysis, C.L.; investigation, C.L.; resources, A.T.; data curation, E.K.; writing—original draft preparation, E.K.; writing—review and editing, I.S.; visualization, C.L.; supervision, T.K.; project administration, T.K. All authors have read and agreed to the published version of the manuscript.

**Funding:** This research is co-financed by Greece and the European Union (European Social Fund-ESF) through the Operational Programme «Human Resources Development, Education and Lifelong Learning 2014–2020» in the context of the project “Magnetic driving of nanoparticles in human arteries” networks (MIS: 5048923).

**Institutional Review Board Statement:** Not applicable.

**Informed Consent Statement:** Not applicable.

**Data Availability Statement:** The data presented in this study are available in the displayed figures and tables within the article, but can also be obtained on request from the corresponding author within a reasonable time-frame.

**Acknowledgments:** The authors would like to acknowledge the support of the Greek Research and Technology Network (GRNET) for the computational time granted in the National HPC facility ARIS.

**Conflicts of Interest:** The authors declare no conflict of interest.

## References

1. Senyei, A.; Widder, K.; Czerlinski, C. Magnetic guidance of drug carrying micro-spheres. *Appl. Phys.* **1978**, *49*, 3578–3583. [[CrossRef](#)]
2. Widder, K.; Senyei, A.; Scarpelli, G. Magnetic microspheres: A model system of site specific drug delivery in vivo. *Proc. Soc. Exp. Biol. Med.* **1978**, *158*, 141–146. [[CrossRef](#)] [[PubMed](#)]

3. Patra, J.K.; Das, G.; Fraceto, L.F.; Campos, E.V.R.; Rodriguez-Torres, M.; Acosta-Torres, L.S.; Diaz-Torres, L.A.; Swamy, M.K.; Sharma, S.; Habtemariam, S.; et al. Nano based drug delivery systems: Recent developments and future prospects. *J. Nanobiotechnol.* **2018**, *16*, 71. [[CrossRef](#)]
4. Arias, L.S.; Pessan, J.P.; Vieira, A.P.M.; Toito de Lima, T.M.; Delbem, A.C.B.; Monteiro, D.R. Iron Oxide Nanoparticles for Biomedical Applications: A Perspective on Synthesis, Drugs, Antimicrobial Activity, and Toxicity. *Antibiotics* **2018**, *7*, 46. [[CrossRef](#)] [[PubMed](#)]
5. Ali, A.; Zafar, H.; Zia, M.; Haq, I.U.; Phull, A.R.; Ali, J.S.; Hussain, A. Synthesis, characterization, applications, and challenges of iron oxide nanoparticles. *Nanotechnol. Sci. Appl.* **2016**, *9*, 49–67. [[CrossRef](#)]
6. Giustini, A.J.; Petryk, A.A.; Cassim, S.M.; Tate, J.A.; Baker, I.; Hoopes, P.J. Magnetic nanoparticle hyperthermia in cancer treatment. *Nano LIFE* **2010**, *1*, 17–32. [[CrossRef](#)]
7. Daughton, C.G.; Ruhoy, I.S. Lower-dose prescribing: Minimizing “side effects” of pharmaceuticals on society and the environment. *Sci. Total Environ.* **2013**, *443*, 324–337. [[CrossRef](#)] [[PubMed](#)]
8. Mao, X.; Xu, J.; Cui, H. Functional Nanoparticles for Magnetic Resonance Imaging. *Wires Nanomed. Nanobiotechnol.* **2016**, *8*, 814–841. [[CrossRef](#)] [[PubMed](#)]
9. Gleich, B.; Hellwig, N.; Bridell, H.; Jurgons, R.; Seliger, C.; Alexiou, C.; Wolf, B.; Weyh, T. Design and evaluation of magnetic fields for nanoparticle drug targeting in cancer. *IEEE Trans. Nanotechnol.* **2007**, *6*, 164–169. [[CrossRef](#)]
10. Kubo, T.; Sugita, T.; Shimose, S.; Nitta, Y.; Ikuta, Y.; Murakami, Y.T. Targeted delivery of anticancer drugs with intravenously administered magnetic liposomes in osteosarcoma-bearing hamsters. *Int. J. Oncol.* **2000**, *17*, 309–315. [[CrossRef](#)] [[PubMed](#)]
11. Yellen, B.B.; Forbes, Z.G.; Halverson, D.S.; Fridman, G.; Barbee, K.A.; Chorny, M.; Levy, R.; Friedman, G. Targeted drug delivery to magnetic implants for therapeutic applications. *J. Magn. Magn. Mater.* **2005**, *293*, 647–654. [[CrossRef](#)]
12. Karvelas, E.G.; Lampropoulos, N.K.; Karakasidis, T.E.; Sarris, I.E. A computational tool for the estimation of the optimum gradient magnetic field for the magnetic driving of the spherical particles in the process of cleaning water. *Desalin. Water Treat.* **2017**, *99*, 27–33. [[CrossRef](#)]
13. Mathieu, J.B.; Martel, S. Aggregation of magnetic microparticles in the context of targeted therapies actuated by a magnetic resonance imaging system. *J. Appl. Phys.* **2009**, *106*, 044904. [[CrossRef](#)]
14. Vartholomeos, P.; Mavroidis, C. In silico studies of magnetic microparticle aggregations in fluid environments for MRI-guided drug delivery. *IEEE Trans. Biomed. Eng.* **2012**, *59*, 3028–3038. [[CrossRef](#)]
15. Karvelas, E.G.; Lampropoulos, N.K.; Sarris, I.E. A numerical model for aggregations formation and magnetic driving of spherical particles based on OpenFOAM. *Comput. Methods Programs Biomed.* **2017**, *142*, 21–30. [[CrossRef](#)] [[PubMed](#)]
16. Karvelas, E.G.; Karakasidis, T.E.; Sarris, I.E. Computational analysis of paramagnetic spherical Fe<sub>3</sub>O<sub>4</sub> nanoparticles under permanent magnetic fields. *Comput. Mater. Sci.* **2018**, *154*, 464–471. [[CrossRef](#)]
17. Karvelas, E.G.; Lampropoulos, N.K.; Benos, L.T.; Karakasidis, T.E.; Sarris, I.E. On the magnetic aggregation of Fe<sub>3</sub>O<sub>4</sub> nanoparticles. *Comput. Methods Programs Biomed.* **2021**, *178*, 105778. [[CrossRef](#)]
18. Fogelson, A.L.; Neeves, K.B. Fluid Mechanics of Blood Clot Formation. *Annu. Rev. Fluid Mech.* **2015**, *47*, 377–403. [[CrossRef](#)]
19. Jackson, J.D. *Classical Electrodynamics*, 3rd ed.; Wiley: Hoboken, NJ, USA, 1998.
20. Agiotis, L.; Theodorakakos, I.; Samothrakitis, S.; Papazoglou, S.; Zergioti, I.; Raptis, Y.S. Magnetic manipulation of superparamagnetic nanoparticles in a microfluidic system for drug delivery applications. *J. Magn. Magn. Mater.* **2016**, *401*, 956–964. [[CrossRef](#)]
21. Hedayatnasab, Z.; Abnisa, F.; Daud, W.M.A.Q. Review on magnetic nanoparticles for magnetic nanofluid hyperthermia application. *Mater. Des.* **2017**, *123*, 174–196. [[CrossRef](#)]
22. Cervadoro, A.; Giverso, C.; Pande, R.; Sarangi, S.; Preziosi, L.; Wosik, J.; Brazdeikis, A. Design Maps for the Hyperthermic Treatment of Tumors with Superparamagnetic Nanoparticles. *PLoS ONE* **2013**, *8*, e57332. [[CrossRef](#)]
23. Myrovali, E.; Maniotis, N.; Samaras, T.; Angelakeris, M. Spatial focusing of magnetic particle hyperthermia. *Nanoscale Adv.* **2020**, *2*, 408–416. [[CrossRef](#)]
24. Simeonidis, K. In-situ particles reorientation during magnetic hyperthermia application: Shape matters twice. *Sci. Rep.* **2016**, *6*, 38382. [[CrossRef](#)]
25. Numata, S.; Itatani, K.; Kawajiri, H.; Yamazaki, S.; Kanda, K.; Yaku, H. Computational fluid dynamics simulation of the right subclavian artery cannulation. *J. Thorac. Cardiovasc. Surg.* **2017**, *154*, 480–487. [[CrossRef](#)] [[PubMed](#)]
26. Arjunan, A.; Demetriou, M.; Baroutaji, A.; Wang, C. Mechanical performance of highly permeable laser melted Ti6Al4V bone scaffolds. *Behav. Biomed. Mater.* **2020**, *102*, 103517. [[CrossRef](#)]
27. Erisken, C.; Tsiantis, A.; Papatthanasasiou, T.D.; Karvelas, E.G. Collagen fibril diameter distribution affects permeability of ligament tissue: A computational study on healthy and injured tissues. *Comput. Methods Programs Biomed.* **2020**, *196*, 105554. [[CrossRef](#)]
28. Zhang, X.; Le, T.A.; Hoshidar, A.K.; Yoon, J. A Soft Magnetic Core can Enhance Navigation Performance of Magnetic Nanoparticles in Targeted Drug Delivery. *IEEE/ASME Trans. Mechatron.* **2018**, *23*, 1573–1584. [[CrossRef](#)]
29. Pouponnea, P.; Leroux, J.-C.; Soulez, G.; Gaboury, L.; Martel, S. Co-encapsulation of magnetic nanoparticles and doxorubicin into biodegradable microcarriers for deep tissue targeting by vascular MRI navigation. *Biomaterials* **2011**, *32*, 3481–3486. [[CrossRef](#)] [[PubMed](#)]
30. Zhang, X.; Le, T.A.; Yoon, J. Development of a real time imaging-based guidance system of magnetic nanoparticles for targeted drug delivery. *J. Magn. Magn. Mater.* **2017**, *427*, 345–351. [[CrossRef](#)]

31. Martel, S.; Felfoul, O.; Mathieu, J.-B.; Chanu, A.; Tamaz, S.; Mohammadi, M.; Mankiewicz, M.; Tabatabaei, N. MRI-based Medical Nanorobotic Platform for the Control of Magnetic Nanoparticles and Flagellated Bacteria for Target Interventions in Human Capillaries. *Int. J. Robot. Res.* **2009**, *28*, 1169–1182. [[CrossRef](#)]
32. kafash, A.; Le, T.A.; Yoon, J. Swarm of magnetic nanoparticles steering in multi-bifurcation vessels under fluid flow. *J. Micro-Bio Robot.* **2020**, *16*, 137–145.
33. Tao, R.; Huang, K. Reducing blood viscosity with magnetic fields. *Phys. Rev. E* **2011**, *84*, 011905. [[CrossRef](#)] [[PubMed](#)]
34. Waite, L. *Biofluid Mechanics in Cardiovascular Systems*; McGraw-Hill's: New York, NY, USA, 2005.
35. Hansen, N. The CMA evolution strategy: A comparing review. *Adv. Estim. Distrib. Algorithms* **2006**, *192*, 1769–1776.
36. Weller, H.G.; Tabor, G.; Jasak, H.; Fureby, C. A tensorial approach to computational continuum mechanics using object-oriented techniques. *Comput. Phys.* **2010**, *12*, 620–631. [[CrossRef](#)]
37. Kennedy, P.; Zheng, R. *Flow Analysis of Injection Molds*; Hanser: New York, NY, USA, 2013.
38. Bharadvaj, B.K.; Mabon, R.F.; Giddens, D.P. Steady flow in a model of a human carotid bifurcation. Part 1-Flow visualization. *J. Biomech.* **1982**, *15*, 349–362. [[CrossRef](#)]
39. Geuzaine, C.; Remacle, J.-F. Gmsh: A 3-D finite element mesh generator with built-in pre- and post-processing facilities. *Int. J. Numer. Methods Eng.* **2009**, *79*, 1309–1331. [[CrossRef](#)]
40. Gijssen, F.J.H.; Vosse, F.N.V.; Janssen, J.D. The influence of the non-Newtonian properties of blood on the flow in the large arteries: Steady flow in a carotid bifurcation model. *J. Biomech.* **1999**, *32*, 601–608. [[CrossRef](#)]
41. Nowogrodzki, A. The world's strongest MRI machines are pushing human imaging to new limits. *Nature* **2018**, *563*, 24–26. [[CrossRef](#)]
42. Segadal, L.; Matre, K. Blood velocity distribution in the human ascending aorta. *Circulation* **1987**, *76*, 90–100. [[CrossRef](#)]
43. Pomella, N.; Wilhelm, E.N.; kolyva, C.; Gonzalez-Alonso, J.; Rakobowchuk, M.; Khir, A.W. Common carotid artery diameter, blood flow velocity and wave intensity responses at rest and during exercise in young healthy humans: A reproducibility study. *Ultrasound Med. Biol.* **2017**, *43*, 943–957. [[CrossRef](#)]
44. Koutsiaris, A.G.; Tachmitzi, S.V.; Papavasileiou, P.; Batis, N.; Koutoula, M.G.; Giannoukas, A.D.; Tsironi, E. Blood velocity pulse quantification in the human conjunctival pre-capillary arterioles. *Microvasc. Res.* **2010**, *80*, 202–208. [[CrossRef](#)] [[PubMed](#)]
45. Griese, F. Simultaneous Magnetic Particle Imaging and Navigation of large superparamagnetic nanoparticles in bifurcation flow experiments. *J. Magn. Magn. Mater.* **2020**, *498*, 166206. [[CrossRef](#)]
46. Manshadi, M.K.D. Delivery of magnetic micro/nanoparticles and magnetic-based drug/cargo into arterial flow for targeted therapy. *Drug Deliv.* **2018**, *25*, 1963–1973. [[CrossRef](#)]
47. Grosse-Wortmann, L.; Grabitz, R.; Seghaye, M.C. Magnetic Guide-Wire Navigation in Pulmonary and Systemic Arterial Catheterization: Initial Experience in Pigs. *J. Vasc. Interv. Radiol.* **2007**, *18*, 545–551. [[CrossRef](#)] [[PubMed](#)]